Detecting the Localization of Defects Using a Coherent Point Drift Algorithm for Robotic Deburring Tasks

Chih-Jer Lin, Ting-Yi Sie

***Abstract*—Work pieces usually have burrs after machining processes. The burrs could result in a potential dimension error and they may cause the impression of following assembly processes. Therefore, the deburring process is very important for casting parts to guarantee the dimension accuracy and surface quality. Many factories still rely on the manual deburring for achieving a suitable quality of product. The reason is because the deburring machine can handle a specified part and it is not feasible for various parts. The manual deburring is highly time-consuming with danger. In addition, the resulting dust and physical demands ultimately represent a health risk. Most typical deburring techniques are applied for the fixed part and it is not easy to be automated. They require many setup processes as different positions are requested deburring for different parts. To improve the surface treatment of deburring parts, how to automate the deburring operation is a important issue in the development of manufacturing. In this study, to detect the burring size and position of a casting, a Realsense F200 camera is used to capture the 3D geometric model to establish a point cloud model. Then, a coherent point drift algorithm based on a variable ROI is proposed to detect burring dimension and location. After that, an automated deburring system is developed by using an UR3 robot integrated with the self-developed automatic optical inspection system.**

***Index Terms*—point cloud, 3D vision, Coherent point drift algorithm**

I. Introduction

Robotics research focuses on trying to solve the problem of uncertainty, one of which is the manipulation of objects in 3D space. The 3D vision of robotics has been a main topic of discussion in recent years and scientists around the world have added different vision systems to their robots in order to improve the ability of robots to perform tasks. [1] On one hand, the function of the robot vision system focuses on the measurement of the pose of the workpiece to guide the robot motion mainly. On the other hand, the robot vision system is used for the three-dimensional attitude measurement of the workpiece. Lindner et al. proposed a novel robot vision system that uses dynamic laser triangulation to determine the three-dimensional (3D) coordinates of the observed object. [2] According to the classification task of the assembly line, Qin et al. designed the industrial robot classification system based on the 3D vision to identify the workpiece and calculate its center coordinate with respect to the robot frame; then the robot can accurately grasp and classify artifacts based on the measurement of the vision system. The robot vision system is usually used to guide the robot motion. Šuligoj et al. proposed a method of relative displacement of the framework and described a multi-robot co-working application that can be used to track, process, or process operations using stereoscopic vision in an unstructured laboratory environment. One robot arm carries a stereovision camera system, and the other has a marker for navigation between the robot and the workpiece. Although this approach has served its purpose, overall hardware costs are still relatively high [3]. In order to improve the efficiency in the production of shoes using robots, Wu et al. proposed a shoe slot's tracking method based on robotic system [4]. The proposed method is mainly to simplify feature extraction by projecting geometric information from 3D to 2D, so as to identify the longest groove feature line in two-dimensional space. When a two-dimensional slot line is detected, it is projected into three-dimensional space to identify the feature point set of the 3D slot [5,6]. In this paper, an automatic detection of a casting's burr is studied using the 3D point cloud technology. The burr detection is performed to compare the golden sample of a STL model from the measured point could models using the F200 camera. The coherent point drift (CPD) algorithm and iterative closest point (ICP) algorithm are used to implement the proposed method.

II. System Description

In this study, a seven DOF redundant robot was developed and used in experiments and simulations. As shown in Figure 1, this robotic arm consists of two control blocks. There are three subsystems; the first one is a six DOF UR3 robot, the second is a rotating stage that make the robot arm rotate, and the final one is the 3D vision system (as shown in Fig. 1 and Table 1). The rotational base stage is actuated by a servo motor (OMRON 1S) and a harmonic drive mechanism (Harmonic drive, CSF-32-100-2A-GR). A real-time controller (OMON NX1P) is used to integrate the UR3 with the rotational stage and this controller is communicated with a PC via the EtherCAT interface. The 6th joint of the UR3 can rotate infinitely and the other joints can rotate 360 degrees; each joint has a force sensing device to ensure operation safety.

The kinematic model of the robot is presented using Denavit-Hartenberg (DH) convention. The set of four parameters for the transformation between two successive frames are denoted by αi, ai,θi, di. As shown in Fig. 2, the UR3 robot is installed on a T-shape struture. According to the coordinate XYZ0 defined in Fig. 2, Table 2 describes the DH parameters of the proposed robot. The first link is actuated by the base servo motor via the harmonic drive mechanism and the UR3 robot provide the next six degrees of freedom (DOFs). Although the robot can be equipped with a gripper attached to its flange, the motion planning with obstacle avoidance is considered without considering the gripper in this study. The forward kinematic relation is used to determine the position and orientation of the end effector given the vector of joint variables.

Then the position and orientation of the end-effector in the ground frame are given by

$$P_0 = A_1 A_2 A_3 A_4 A_5 A_6 A_7 P_7 \quad (1)$$

, where P_7 is a coordinate for a given point is expressed relative to the frame 7; A_i is the ith transformation of coordinate according to the DH table; P_0 is the position and orientation of the end-effector in the inertial frame. If $P_7 = [0\ 0\ 0\ 1]^T$ is substituted into Eq. (1), then we have the forward kinematic function of the robot as follows.

$$\mathrm{r} = \begin{bmatrix} x \\ y \\ z \\ 1 \end{bmatrix} = \boldsymbol{f}(\theta_1, \theta_2, \theta_3, \theta_4, \theta_5, \theta_6, \theta_7) \quad (2)$$

, where (x,y,z) represents the coordinate of the flange center with respect to the world frame.

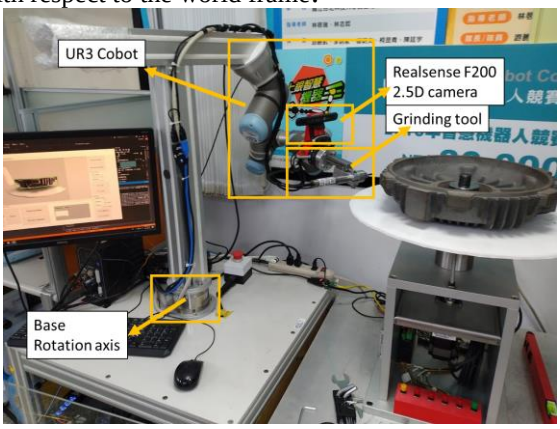

Fig. 1 Proposed system with 3D vision for deburring

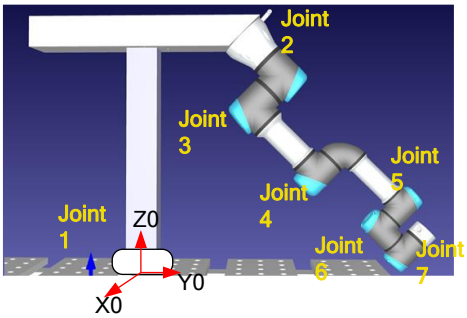

Fig. 2

TABLE I
SPEC LIST OF HARDWARE AND EQUIPMENT USED IN THIS STUDY

Item	Type	Specification
F200	RGBD camera	Depth resolution 640 x 480 working distance 0.2m~1.2m
UR3	6-axis robotic arm	Six-DOF/ Payload 3kg/ Repeat accuracy ±0.1mm

Table II DH table of the proposed robot.

Joint	αi(deg)	ai(mm)	θi(deg)	di(mm)
J1	0	-280	-90	0
J2	135	0.0	0.0	118.0
J3	90	0.0	180.0	0.0
J4	0.0	243.7	0.0	0.0
J5	0.0	213.0	0.0	110.4
J6	-90	0.0	0.0	83.4
J7	90	0.0	180.0	82.4

The motion planning of the proposed robot is developed in MATLAB; then, the motion planning results were transmitted to the NX1P controller (for the rotation stage) and UR3 controller using the C# code via Ethernet. Because the proposed robotic arm has one redundancy to make the motion planning with flexibility, we can switch the motion in the deburring task between multiple poses with using the redundancy. To obtain the 3D information of the deburred object, we installed the Realsense F200 camera at the end of the arm in order to scan the object to be tested through the action of the arm. The camera's real-time scanning information is acquired and integrated using the DF_3DScan GUI. The developed scanning program can extract a complete and accurate output data set with respect to single-shot stereo images, which are used by feature matching and image processing. We developed a C# code to control the robotic motion with a series of paths to capture and calculate the 3D images of the workpiece. After obtaining the orientation of the workpiece, the burr areas are compared by the proposed CPD algorithm to obtain the deburring area. Figure 3 shows the five positions for scanning the 3D profiles of the deburred workpiece. At the first step, the 3D profile of the normal workpiece is captured using Realsense F200 camera. Then, the five data scanning data sets are integrated into a model of 3D point cloud as the golden model (as shown in Fig. 4).

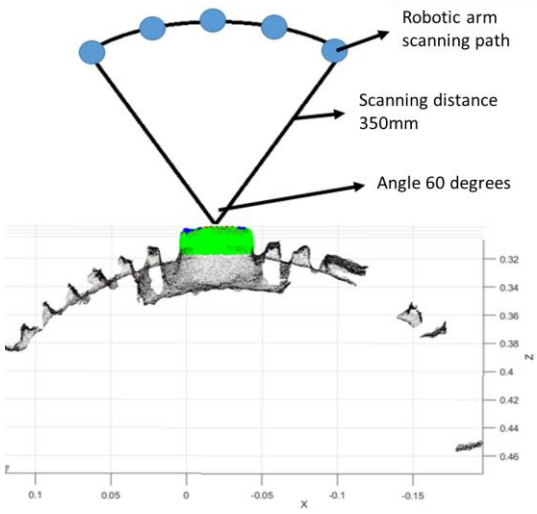

Fig. 3 Scanning motion of the deburring process

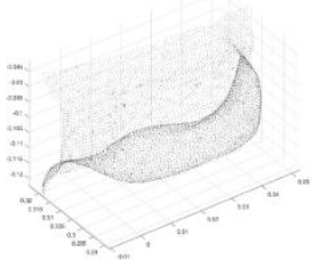

Fig. 4 The good sample with no burr

III. MAIN RESULTS

A. *Point cloud matching based on CPD algorithm*

In order to match the captured 3D cloud image with the golden sample, a CPD algorithm with weighting parameters is used as the main algorithm for matching of point cloud model. The CPD algorithm was proposed by Myronenko in 2005 and was improved in 2010 [7]. The CPD algorithm considers point cloud matching as an estimate of the probability density. CPD uses the Gaussian mixture model (GMM) to solve the matching relationship. There are two main advantages of CPD, which are setting with the suitable weighting parameter can improve the anti-noise ability for matching and iterations of CPD algorithm can improve its performance of model matching.

The CPD algorithm considers point cloud matching as an estimate of the probability density. CPD uses the Gaussian mixture model (GMM) to solve the registration relationship. If $Y_{M\times D} = (y_1,\cdots,y_M)^T$ represents the point cloud of the good part with using a vector containing the coordinates of the N boundary points, where correspondences are represented by a Gaussian Mixture Model (GMM) and target points are considered as the centers of the Gaussian mixtures and D represents the dimension. If the measured point cloud set of the workpiece using the Realsense F200 camera is denoted by $X_{N\times D} = (x_1,\cdots,x_N)^T$, then the registration process of the CPD algorithm is like the Expectation-Maximization (EM) algorithm to estimate correspondences in the E-step and to update the trans-formation in the M-step [8]. The EM algorithm is an iterative method to find maximum a posteriori or maximum likelihood estimates of parameters in statistical models using Bayes theorem. The basic EM Paradigm of the CPD can be described as follows.

(1) Initialization: Given initial guess of registration to compute the variance of distances between all possible point pairs. Then, the independent isotropic Gaussian distribution is assumed for matches and a uniform distribution for outliers [8].

(2) In the E-step, the likelihood function is calculated using the current estimates of parameters. Based on current variance, the CPD algorithm computes probability of matches of all possible point pairs to decide what are outliers

(3) In the M-step, the parameters maximizing the likelihood function are calculated and the process iterates until convergence. In order to solve correspondence problem, the CPD algorithm computes new transformation that increases probability and update probabilities based on registration.

(4) The target points are considered as the centroids of a GMM and they are fitted to the measured point cloud set of the workpiece through maximizing the likelihood function of the reference points. The E-step is used to find the maximum likelihood function, which is calculated using the current positions of the target points. The M-step is used to find the new positions of the centers that maximize the likelihood function are estimated. This algorithm is guaranteed to converge from almost any initial condition [9].

B. *Burr detection with the CPD algorithm*

Table 3 describes the notations and meanings of the variables used in this article. To detect the burr of the part, the measured GMM model of the measured workpiece ($X_{N\times D}$) is computed to match the point cloud set $Y_{M\times D}$ (the GMM centroid of the good part) using the rigid point set registration[7]. Then, we can find the different point set between the measured part and the good part to find the position of the burr. The proposed process is separated into three stages to reduce the scope of searching burr gradually and the computing process is shown in Figure 5.

Stage 1: the CPD algorithm is performed for 20 iterations to match the measured point could model and the GMM of the good part. Figure 6 shows the initial relation and the final relation using the CPD for the two models. After the first stage, we can find the transformation matrix T_1, which describes the relation between the point cloud models $X_{N\times D}$ and $Y_{M\times D}$. From the result in Figure 5, it shows that there exists the location error after the first stage of CPD computation.

Stage 2: To speed up the computation time of registration, we define a region of interest (ROI) of the GMM model to reduce the matching error. If $T_1(Y)$ describes the transformation of the first stage, then the filter of the fixed point cloud $X_{N\times D}$ is defined as follows.

$$1.25\min T_1(Y_{x,y}) \le X_{N\times D} \le 1.25\max T_1(Y_{x,y}) \qquad (1)$$

, where $\min T_1(Y_{x,y})$ is the minimal value of the first transformation $T_1(Y)$ and $\max T_1(Y_{x,y})$ is the minimal value of the first transformation $T_1(Y)$ of the volume in x and y direction. After reducing the set $X_{N\times D}$ by the ROI filter, we can find the second transformation matrix T_2. The CPD algorithm is performed for 20 iterations to match the measured point could model and the second GMM.

Stage 3: To increase the accuracy of the location for the CPD computation, we define a region of interest (ROI) of the GMM model for the third pattern matching process. The filter of the fixed point cloud $X_{N\times D}$ for the third stage is defined as follows.

$$\min T_2T_1(Y_{x,y}) \le X_{N\times D} \le \max T_2T_1(Y_{x,y}) \qquad (2)$$

Figure 7 shows the results using the CPD with different ROI for the above three stages. The results show that the proposed CPD method with various ROI can make the measured point cloud set match the GMM of the good part efficiently.

After three stages of CPD computations, we can make the GMM model of the good part be allocated to the measured 3D could data as shown in Fig. 8. Figure 9 shows the difference between the golden sample and the measured results, where the green part represents the model of the good sample and the red is the actual measured point cloud set obtained by the proposed robotic measurement system. In order to reduce the computation loading for the curved surface on the left in Fig. 10, we apply the proposed method using the small ROI before calculating the amount of burr. The burr's location can be computed according to the distance between the two point-cloud sets and the different areas are highlighted in Figure 11. In Figure 11, the

blue defect points are the location with a distance greater than 0.6mm. Therefore, the burr location can be found for the robotic deburring task.

TABLE III LIST OF NOTATIONS

Notations	Meanings
D	dimension of the point sets
N, M	number of points in the point sets
$X_{N\times D} = (x_1,...,x_N)^T$	the first point set (the data points)
$Y_{M\times D} = (y_1,...,y_M)^T$	the second point set (the GMM centroids)
$T_n...T_1(Y)$	multiple transformation T applied to Y

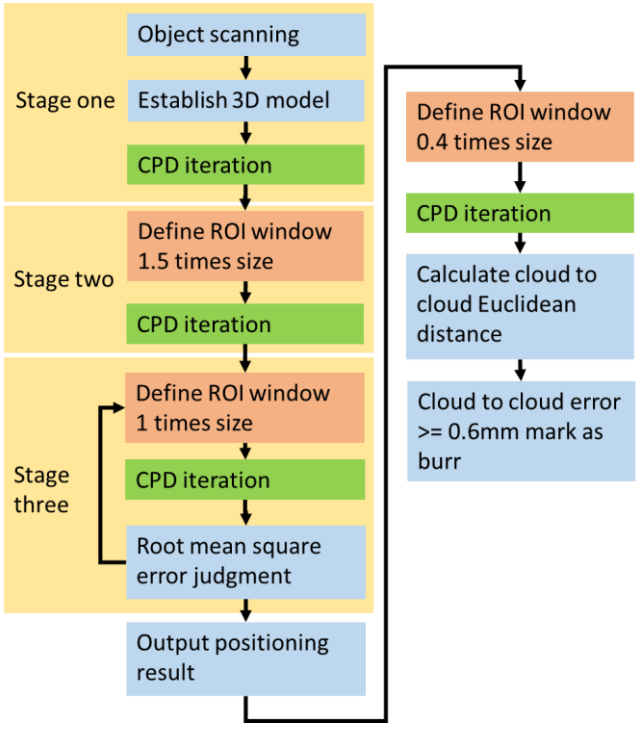

Fig. 5 Flow chart of the CPD algorithm with various ROI

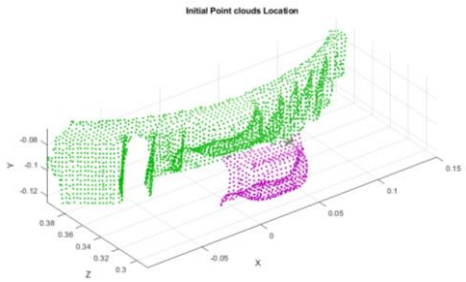

(a) Initial position of the two models

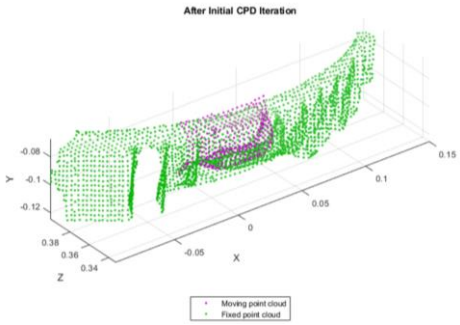

(b) Matching results of the proposed method for 20 iterations

Fig. 6 Matching result of the CPD method in Stage 1

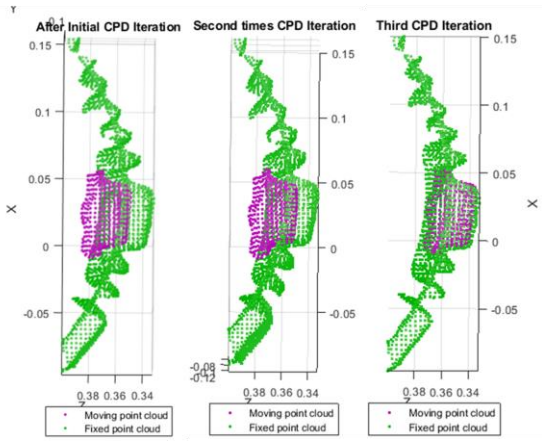

Fig. 7 Results using the CPD iteration with various ROI for three stages

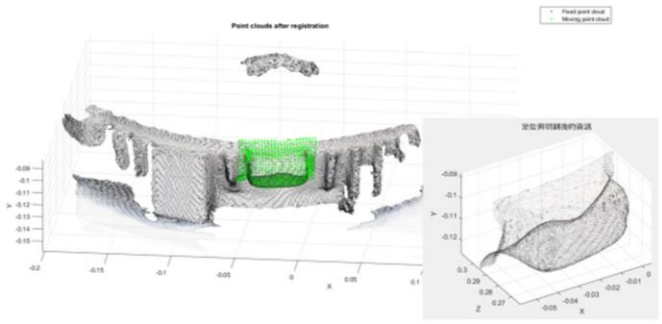

Fig. 8 The final result after three stages using the CPD method

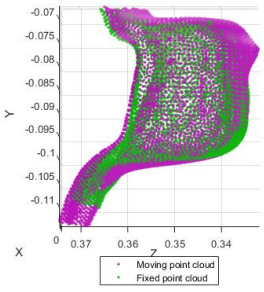

Fig. 9 Comparison between the golden sample and the measured

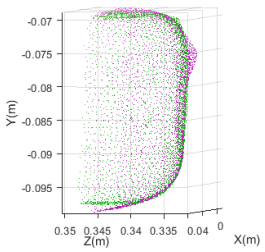

Fig. 10 Comparison between the golden sample and the measured from the Top view

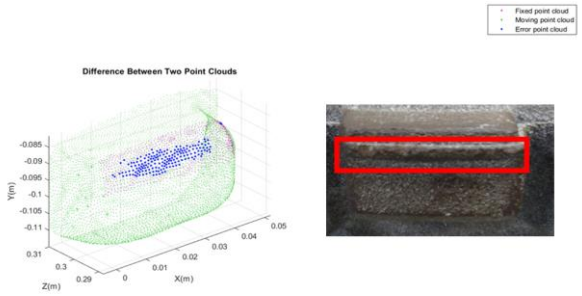

Fig. 11 Registration of the burr region using the proposed method

IV. Case Studies and Discussion

To compare the results using the ICP algorithm with the CPD algorithm, we divide the four-stage point set matching in Fig.5 into two stages, which the first stage is used to discuss the accuracy of location and the second is used for the calculation of the burrs. The purpose of Stages 1~3 in Section 3 is used to locate the measured pattern on the surface of the workpiece quickly. The matching point set used at this time is down-sampled to improve computing efficiency. After positioning through the down-sampled point set, the positioning result is output to the right block of Fig. 5 for detailed error calculation. In Figure 5, each of the three stages of positioning takes 20 iterations, a total of 60 iterations. After 60 iterations, the last 20 detailed iterations are performed to calculate the calculation of the burr points. The overall process costs a total of 80 iterations.

The specifications of the computer used for this experiment are CPU: Intel(R)Xeon(R)CPU X5647 2.93GHz, and memory: DDR3 72GB. To compare the root mean square value of the Euclidean distance between the point set and the point set after each matching stage and the calculation time of each stage using the different algorithms, four cases are designed to compare the computation performance of the different algorithms.

The first case uses the CPD algorithm for obtaining the burr location in Stage 1-3 and the CPD algorithm is used for the detailed iteration in the last stage. Table IV shows the distance error and computation time for the (CPD/CPD) method. The second case uses the ICP algorithm for obtaining the burr location in Stage 1-3 and the ICP algorithm is used for the detailed iteration in the last stage. Table V shows the distance error and computation time for the (ICP/ICP) method. The third case uses the ICP algorithm for obtaining the burr location in Stage 1-3 and the CPD algorithm is used for the detailed iteration in the last stage. Table VI shows the distance error and computation time for the (ICP/CPD) method. The fourth case uses the CPD algorithm for obtaining the burr location in Stage 1-3 and the ICP algorithm is used for the detailed iteration in the last stage. Table VII shows the distance error and computation time for the (CPD/ICP).

From the experimental results of Table IV, it can be seen that as the positioning ROI of each stage shrinks, the RMS error between the two point sets is gradually reduced. According to the calculation time for Stage 1-3 (60 iteration), the iteration time of each stage is significantly reduced if the matching method with various ROI is achieved. Besides of reducing the calculation time, the distance error of matching two models is also decreased and the location of burr zone can be found finally.

With comparing Table IV and Table V, if matching error is concerned, the ICP method has the smaller RMS error than the CPD in the first and second stages, but the CPD has the smaller RMS error than the ICP in the third stage. Based on the purpose of looking for burrs, it is necessary to reduce the iteration error as much as possible when the two point sets are partially different. In this case, the probability-based CPD algorithm is better than the conventional ICP algorithm. However, according to the computation time of the fourth stage, the CPD algorithms need more time than the ICP algorithms. If the computation time of the CPD algorithm is acceptable, the proposed CPD method with multiple stages using different ROI zones have the ability to find the burr location for the robotic deburring tasks.

TABLE IV
Method CPD/CPD

Method CPD /CPD	Iteration 0-20	Iteration 20-40	Iteration 40-60	Iteration 60-80
distance error (mm)	41.936	6.774	1.826	0.677
Time (sec)	0.382	0.081	0.083	2.238

TABLE V
Method ICP/ICP

Method ICP /ICP	Iteration 0-20	Iteration 20-40	Iteration 40-60	Iteration 60-80
distance error (mm)	2.998	2.415	2.240	1.086
Time (sec)	0.287	0.044	0.026	0.055

TABLE VI
Method ICP/CPD

Method ICP /CPD	Iteration 0-20	Iteration 20-40	Iteration 40-60	Iteration 60-80
distance error (mm)	2.998	2.415	2.240	0.615
Time (sec)	0.260	0.042	0.025	2.208

TABLE VII
METHOD CPD/ICP

Method CPD /ICP	Iteration 0-20	Iteration 20-40	Iteration 40-60	Iteration 60-80
distance error (mm)	41.936	6.774	1.826	0.681
Time (sec)	0.378	0.082	0.083	0.115

V. CONCLUSION

This paper proposes a point cloud matching method with dynamic ROI area to search for defects in the workpiece. It can gradually reduce the root mean square error of iterative calculation without manually adjusting the weight value. Dynamic ROI makes it tolerant of small deviations in workpiece processing. With comparing the ICP algorithm with the CPD algorithm, the point cloud set matching are discussed in four case studies. With comparing Table IV and Table V, if matching error is concerned, the ICP method has the smaller RMS error than the CPD in the first and second stages, but the CPD has the smaller RMS error than the ICP in the third stage and the final stage. However, according to the computation time of the fourth stage, the CPD algorithms need more time than the ICP algorithms. If the computation time of the CPD algorithm is acceptable, the proposed CPD method with multiple stages using different ROI zones have the ability to find the burr location. Therefore, the proposed method can locate the burr zone of the metal part for the robotic deburring tasks.

ACKNOWLEDGMENT

The authors would like to thank the National Science Council of the Republic of China, Taiwan, for financially supporting this research under Contract No. MOST 107-2221-E-027-116 and 107-2218-E-027-018.

REFERENCES

[1] Andreopoulos, A.; Tsotsos, J.K. 50 Years of object recognition: Directions forward. Comput. Vis. Image Underst.2013, 117, 827–891.
[2] Lindner, L.; Sergiyenko, O.; Rodríguez-Quiñonez, J.C.; Rivas-Lopez, M.; Hernandez-Balbuena, D.;Flores-Fuentes, W.; Natanael Murrieta-Rico, F.; Tyrsa, V. Mobile robot vision system using continuous laser scanning for industrial application. Ind. Robot Int. J. 2016, 43, 360–369.
[3] Šuligoj, F.; Šekoranja, B.; Švaco, M.; Jerbi´c, B. Object tracking with a multiagent robot system and a stereo vision camera. Procedia Eng. 2014, 69, 968–973.
[4] Wu, X.; Li, Z.;Wen, P. An automatic shoe-groove feature extraction method based on robot and structural laser scanning. Int. J. Adv. Rob. Syst. 2016, 14.
[5] Fitzgibbon, A.W. Robust registration of 2D and 3D point sets. Image Vis. Comput. 2003, 21, 1145–1153.
[6] Aldoma, A.; Vincze, M.; Blodow, N.; Gossow, D.; Gedikli, S.; Rusu, R.B.; Bradski, G. CAD-model recognition and 6DOF pose estimation using 3D cues. In Proceedings of the 2011 IEEE International Conference on Computer Vision Workshops (ICCVWorkshops), Barcelona, Spain, 6–13 November 2011; pp. 585–592.
[7] Myronenko, Andriy, and Xubo Song. Point set registration: Coherent point drift. IEEE transactions on pattern analysis and machine intelligence 32.12 (2010): 2262-2275.
[8] Delavari, M., Foruzan, A. H and Chen, Y.W. Accurate point correspondences using a modified coherent point drift algorithm. Biomedical Signal Processing and Control 52 (2019): 429-444.
[9] Chui, H., Rangarajan, A. A new point matching algorithm for non-rigid registration, Comput. Vision Image Understanding 89 (2003): 114–141.

Chih-Jer Lin received the B.S., M.S., and Ph.D. degrees from National Cheng Kung University, Tainan, Taiwan, in 1992, 1994, and 1998, respectively, all in mechanical engineering. He is currently a Professor and the Director of the Graduate Institute of Automation and Technology, National Taipei University of Technology. His current research interests include mechatronics, precision motion control, system identification, sliding-mode control, robotics, and evolutionary algorithms.

Ting-Yi Sie received his B.S. degree in Electrical Engineering from the National Taipei University of Technology in 2017. In the same year, he enrolled at Graduate Institute of Automation Technology for master's degree. He is a Ph.D. student in the Graduate Institute of Automation Technology, National Taipei University of Technology until 2019. His current researches include robotic arms, stereo vision and computer-aided system integration.